Structure of Randomly Cross-Linked Poly(dimethylsiloxane) Networks Produced by Electron Irradiation

A. N. Falcão,*,† J. Skov Pedersen, and K. Mortensen

Department of Solid State Physics, Risø National Laboratory, DK-4000 Roskilde, Denmark

Received March 24, 1993; Revised Manuscript Received July 9, 1993•

ABSTRACT: The structure of randomly cross-linked poly(dimethylsiloxane) networks is studied as a function of cross-link density. The networks are produced by irradiating a polydisperse polymer melt with 10-MeV electrons. Average molecular weights in between elastically effective links are obtained from macroscopic equilibrium swelling measurements that are interpreted in the framework of classical *phantom* network models. The values agree with results from a statistical approach based on the Flory–Stockmayer theory assumptions for the cross-linking process. Small-angle neutron scattering measurements were performed on polymer networks swollen to equilibrium in deuterated solvent and on polymer solutions. The scattering from the swollen networks is interpreted by introducing a model that describes the density fluctuations in the swollen network as being fractal at large length scales. The fractal dimension is $^5/_3$. The correlation length of the large-scale density fluctuations is related, through a scaling relation, to the number of monomers in between elastically effective cross-links obtained from the macroscopic swelling measurements and the statistical approach.

1. Introduction

Cross-linking polymer chains creates, above a certain cross-link density, a macroscopic network of connected polymers. An elastomer is formed and the properties of the system change from liquid-like behavior to solid-like behavior. A complete understanding of the physical properties of the system aims at obtaining quantitative relations between the properties and the structural characteristics that determine them. In the case of a polymer network, the cross-links constitute the important molecular feature that determines the microscopic structure upon which depend the physical properties.[1–3] Their number and spatial distribution determine the average molecular weight in between cross-links, M_c, and the distribution about this average.

Polymer networks and gelation processes have been an active area of research for many years. Nevertheless there are a number of questions related to network structure which have not yet been completely understood.

Classical network models,[4,5] based on the assumption that the network strands in between cross-links conform according to Gaussian statistics and that the macroscopic deformation results from the deformation of the individual chains, give a reasonably good account of the macroscopic properties of polymer networks. Difficulties in the quantitative interpretation of experimental results of stress–strain measurements performed on dry networks or equilibrium swelling measurements in a solvent have been attributed to the presence of defects in the network.

To test the different models, an *a priori* knowledge of the network structure is needed. This can only be achieved by knowing the exact distribution of the cross–links and the conformation of the system before the cross-linking process. Presently this is not possible and defect structures like dangling ends, trapped entanglements, or inhomogeneities will be present and difficult to account for. Considerable effort has been put in producing the so-called *model networks*, networks having controllable and independently known structural characteristics.[12,13] But even the model networks are not free of defects. Although it is possible to have a reasonable control over the number of dangling ends, it is however impossible to know the amount of loops and trapped entanglements. Loops are expected, in particular, when the networks are prepared by cross-linking solutions with low polymer concentration or when the molecular weight of the precursor polymer is low.[14,15] Trapped entanglements will be present in networks when the polymer concentration in the state of preparation is high.[16] This is naturally enhanced when the cross-linking is performed in the dry state.

Different improvements to the original models have been proposed to account for the presence of defects,[6–11] without solving all the difficulties in explaining the experimental data.

Information concerning the microscopic structure of the networks can be obtained by the use of scattering techniques. Due to the length scales involved and the possibility of selective deuteration of polymer chains (and/or solvent, when present), small-angle neutron scattering constitutes a particularly powerful tool to investigate the local conformation of the polymer chains and how the conformation changes upon macroscopic deformation. Experiments performed on systems with mixtures of deuterated and protonated chains have shown that the radius of gyration and the local conformation of the polymeric chains are not affected by the cross-linking process, especially when it is performed in the dry state.[17,18] In the dry state the network chains conform according to a random walk like in the polymer melt, giving support to the starting assumption of the classical models. But scattering studies have also shown[18–20] that the local conformation of each chain is little changed when the network is swollen to very different swelling ratios $Q = V/V_0$, where V and V_0 represent the swollen and the dry volume of the network, respectively. This is in contrast with the classical picture of regular expansion of the network upon deformation and led to the suggestion[19] that different mechanisms have to be considered to explain how a macroscopic change in shape or volume is accommodated at the microscopic level. It is well documented now that the classical models are not able to explain the scattering pattern of networks[19,21,22] (either stretched or swollen), and the discrepancies seem far too many to be explained only by the presence of defect structures.

† On leave from Laboratório Nacional de Engenharia e Tecnologia Industrial, Sacavém, Portugal.

• Abstract published in *Advance ACS Abstracts*, September 1, 1993.

0024-9297/93/2226-5350$04.00/0

Recently a model[23,24] derived from an analogy with a percolation problem was proposed to describe the network structure and the microscopic changes that take place when the network is deformed by either stretching or swelling. This model explains general qualitative features of the intensity scattered by gels but predicts some scaling relations which have generally not been observed. It also predicts that the intensity scattered in the limit of zero scattering vector should have a maximum when plotted as a function of cross-link density, and this has never been observed.

The present work reports the structural study of polymer networks swollen to equilibrium and its dependence on cross-link density. The precursor polymer is poly(dimethylsiloxane) (PDMS), and the networks have been produced by irradiating the polymer melt with high-energy electrons, a process that proved to be very reproducible. Samples with cross-link densities covering a very broad range have been studied.

The paper is organized in three main sections. The first section includes the characterization of the molecular weight distribution in the PDMS melt used and the study of the radiation effect on the molecular weight distribution. In the following section results from equilibrium swelling measurements, their interpretation in the framework of classical theories, and a comparison with results from a statistical approach for the linking process are presented. The last section concerns results of small-angle neutron scattering (SANS) measurements performed on polymer solutions and networks swollen to equilibrium. The SANS results reported in this paper are for networks from which the soluble components that remained after irradiation were not extracted.

2. Characterization: Polymer Melt and Networks

A commerially available poly(dimethylsiloxane) with trimethyl termination was used—the PS047 from Hüls-Petrach. According to the catalog information this polymer has a molecular weight of 91 700 and a viscosity of 30 000 centistokes.

2.1. Polymer Melt: Molecular Weight Distribution. The polymer molecular weight distribution was determined by gel permeation chromatography (GPC). The GPC column system consisted of two 50-cm Shodex A-80M columns. The chromatogram was obtained with the system running in toluene at a flow rate of 1 mL/min by injecting 100 μL of a 2.6 mg/mL polymer solution in toluene.

The chromatogram revealed a broad distribution with evidence of a long low molecular weight tail that included a peak in the low limit (Figure 1a). The chromatogram was analyzed using a calibration curve obtained from PDMS standards that were produced for that purpose. The molecular weight corresponding to the main peak of the chromatogram was found to be 91 000, in good agreement with the value 91 700 given by the supplier.

The chromatogram was normalized and converted into a weight distribution using[25]

$$\frac{dH}{dM} = \frac{dH(V)}{dV}\frac{dV}{d\log(M)}\frac{d\log(M)}{dM}\log e \qquad (1)$$

where the first term is the normalized chromatogram height at elution volume V, the second is the inverse slope of the calibration curve at V, and the third is the inverse molecular weight obtained from the calibration curve.

The molecular weight distribution obtained is shown in Figure 1b. The number-average and weight-average

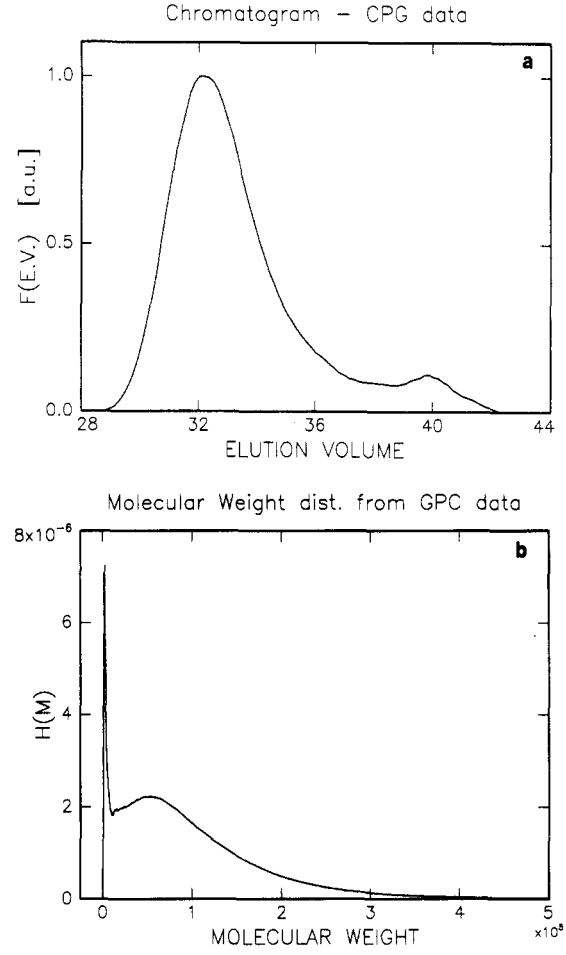

Figure 1. Results of gel permeation chromatography (GPC) performed on the precursor polymer (poly(dimethylsiloxane)) used to produce the networks: (a) chromatogram; (b) molecular weight distribution in the PDMS melt.

molecular weights were calculated from the moments:

$$A_i = \sum_{j=M_{min}}^{M_{max}} H(M)M^{i-1}\Delta M \qquad (2)$$

$$M_n = A_1/A_0, \quad M_w = A_2/A_1 \qquad (3)$$

The values found were $M_n \simeq 16\,000$ and $M_w \simeq 77\,500$, giving the relatively large polydispersity $M_w/M_n \simeq 4.5$.

2.2. Networks: Preparation and Gel Fraction Determination. In the bulk state PDMS is a liquid of polymer chains (*melt*) at room temperature. Irradiating the melt with high-energy electrons randomly creates radicals that, after diffusion processes, react forming chemical links. Above a certain radiation threshold (the *gelling dose*), a macroscopic network of connected polymers spans the whole sample.

For the irradiation the polymer melt was deposited inside flat containers with a cylindrical shape. It was first centrifuged and then allowed to rest until uniform films were obtained. The typical thickness of the films was around 0.5 mm, but samples with thicknesses ranging from 0.3 to 3 mm were also prepared. Before being irradiated, they were kept for at least 12 h under a continuously renewing N_2 atmosphere to remove the oxygen. The samples were then exposed to the 10-MeV electron beam available at the 10-MeV electron accelerator facility of the Risø National Laboratory. To reduce the chain scission probability, the samples were kept under the N_2 atmosphere during irradiation.

The total dose received by each sample was deposited in steps. The steps used changed slightly from sample to

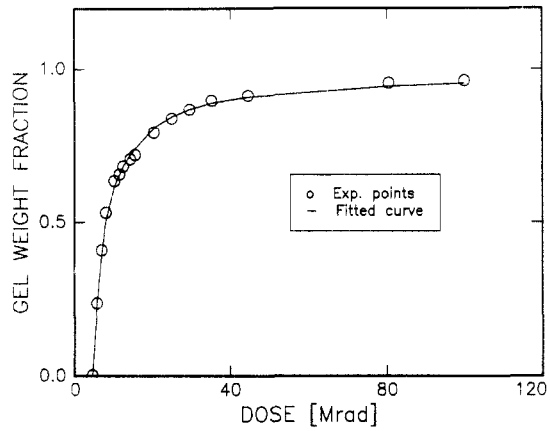

Figure 2. Gel weight fraction dependence on irradiation dose. The open circles represent the experimental points. The full line represents calculated values obtained from eq 4 with a cross-link density $q_0 = 1.9 \times 10^{-4}$ Mrad^{-1} and a ratio between the scission and linking densities $p_0/q_0 = 0.02$. The broad crossover spanning irradiation doses from ~8 to ~40 Mrad is the result of the broad molecular weight distribution in the melt.

sample but were typically around 1 Mrad each.

For the study reported here, more than 50 samples were prepared by this process, using different accelerator runs. As accessed by the study performed, there is no evidence that the structural transformations induced by the radiation depend on the steplike process used to deposit the energy nor on the fact that samples were produced at different times using different accelerator runs. The sample preparation process is very reproducible.

The gel fraction, given by the weight fraction of the initial polymer included in the macroscopic network, was determined for a set of samples irradiated to doses ranging from 3 to 100 Mrad. The extraction of the material not incorporated in the network was performed by immersing the irradiated samples in a continuously renewing bath of *p*-xylene under a N_2 atmosphere for several days. To test the washing process, some of the samples were extracted by simple immersion in an excess of solvent that was periodically renewed (every 2 days in the first 2 weeks, and once a week thereafter). These were kept in the washing bath for more than 2 months.

After the extraction procedure, the remaining material was dried in vacuum at a constant temperature of 60 °C. Some of the samples were also dried at room temperature to check the drying method influence on the experimental gel fractions.

The gel weight fractions showed no dependence on the washing process used nor on the drying method. The experimental results obtained are presented in Table I and represented as a function of irradiation dose in Figure 2 by the open circles. Each point is typically an average of three different measurements.

The shape of the gel fraction curve shows usual features:[30] After the *gelling dose* (estimated from the gel curve to be $r_{gel} \simeq 4.5$ Mrad), the fraction of polymer incorporated in the network increases, approaching a limiting value close to unity. The characteristic steep increase in the gel fraction for the samples studied is slowed down at ca. 8 Mrad, giving rise to a broad crossover to the saturation limit. This is associated with the broad molecular weight distribution and, in particular, with the large amount of low molecular weight material present in the melt.

The very high values the gel fraction attains at high irradiation dose are to be stressed. They suggest a very low scission probability.

The gel fraction curves were analyzed using expressions[26] that describe the gel weight fraction dependence on the irradiation dose. The expressions are the result of a statistical approach based on the Flory–Stockmayer theory assumptions[27-29] relative to the cross-linking process. It is assumed that (i) both cross-linking and scission take place, (ii) the fraction of points that have undergone cross-linking or scission is much less than unity, (iii) end-linking after main-chain scission is negligible, and (iv) intramolecular linking is also negligible. Under these conditions, if p and q are the probabilities that a randomly chosen monomer unit in the system has experienced scission or shares a cross-link, respectively, the gel weight fraction ω_g is given by the implicit equation[26]

$$\omega_g = 2x[1 - (1 - \sum_{P=1}^{\infty} N_P e^{-yP})/y\bar{P}_n] - x^2[1 - 2(1 - \sum_{P=1}^{\infty} N_P e^{-yP})/y\bar{P}_n + 1/\bar{P}_n \sum_{P=1}^{\infty} N_P e^{-yP}] \quad (4)$$

with

$$x = \frac{\omega_g}{p/q + \omega_g} \quad (5)$$

$$y = q(p/q + \omega_g) \quad (6)$$

where N_P is the mole fraction of molecules with degree of polymerization P, $\bar{P}_n = \bar{M}_n/m_0$ is the number-average degree of polymerization, m_0 is the monomer weight, and $\bar{M}_n$ is the number-average molecular weight. The parameters p and q are usually considered to be proportional to the irradiation dose r,[30] i.e., $p = p_0 r$ and $q = q_0 r$, q_0 and p_0 being respectively the cross-link and main-chain scission densities that characterize the efficiency of the radiation for the cross-linking process.

Equation 4 was fitted to the experimental gel fraction points using the molecular weight distribution obtained from the GPC data. All the measured networks were treated simultaneously. Assuming that p and q are proportional to the irradiation dose r, the process used consisted in first computing x and y from eqs 5 and 6, using the experimental gel fractions ω_g^{exp} and values for q_0 and p/q. The calculated x and y and the molecular weight distribution in the original melt were then used to obtain ω_g from eq 4. The values of the parameters q_0 and p/q were varied by performing a least-squares fit.

The starting value for q_0 was $q_0 = 2.1 \times 10^{-4}$ Mrad^{-1}, obtained from the *gelling dose* ($\simeq$4.5 Mrad) and the weight-average molecular weight under the crude assumption that the gel point is reached when there is, on average, one cross-linked unit per weight-average molecule.[30] The first guess for the ratio p/q was obtained from the weight fraction of the material extractable after irradiation, ω_s ($\omega_s = 1 - \omega_g$), plotting[30] $\omega_s + \omega_s^{1/2}$ versus reciprocal dose, and extrapolating to the limit $r^{-1} \to 0$. The value used was $p/q = 0.12$.

The best fit to the experimental data was achieved with $q_0 = 1.95 \times 10^{-4}$ Mrad^{-1} and a ratio $p/q = 0.02$, giving an almost negligible scission probability: $p_0 = 3.9 \times 10^{-6}$ Mrad^{-1}. The values for ω_g (eq 4) that resulted from the fit are presented in Table I and plotted in Figure 2 together with the experimental data. The agreement obtained is very good.

The scission probability q_0 is low as expected from the gel fraction curve, and, as is apparent from Figure 2, even with this low q_0 value, the experimental gel fractions in the samples irradiated to high doses are systematically, although slightly, above the calculated values. However,

Table I. Experimental Gel Weight Fractions and Calculated Values Obtained from Equation 4 with a Cross-Link Density $q_0 = 1.9 \times 10^{-4}$ Mrad^{-1} and a Ratio between the Scission and Linking Densities $p_0/q_0 = 0.02$

dose (Mrad)	gel weight fraction	
	exp	calc
4.76	0.003	0.003
5.93	0.237	0.234
7.11	0.410	0.398
8.15	0.532	0.504
10.35	0.636	0.615
11.61	0.656	0.652
12.57	0.682	0.681
14.41	0.706	0.719
15.65	0.715	0.739
20.49	0.793	0.807
25.09	0.838	0.843
29.66	0.867	0.867
35.41	0.896	0.888
44.72	0.912	0.908
80.61	0.954	0.943
99.98	0.962	0.952

as already mentioned, the different measurements made for each sample produced essentially the same results. The systematic deviation at high dose may be explained by the fact that some of the soluble components are not able to diffuse out of the swollen system. This trapping effect is expected to increase with increasing linking density, and so it should be more evident at high irradiation dose as observed.

For PDMS networks produced by irradiation, the values reported[31] for the ratio between the scission and cross-linking densities come from γ-irradiation and cover a broad range (from negligible up to 0.286), with most of the quoted values lying between 0.08 and 0.25. The p/q ratio obtained is low when compared to these values. However, in γ-irradiation, the exposure times required to deposit the same amount of energy uniformly distributed in the samples are longer, and the control over the sample environment is more difficult to maintain. The relatively low main-chain scission value could be associated with differences that result from the use of different radiations and different irradiation procedures.

It should be noted that the fact that scission is not observed does not mean that it does not take place. In connection to this it has been pointed out[32] that recombination occurs following scission. Some scission products may exchange Si–O bonds with other macromolecules, thus leaving unobserved the full extent of the scission process.

The number of cross-links produced per 100 eV absorbed, $G_{\text{cross-link}}$, is given by[30] $G_{\text{cross-link}} = 0.48 \times 10^6\, q_0/m_0$. The q_0 value obtained in the present work leads to $G_{\text{cross-link}} = 1.2$ links/100 eV. This value is also in the lower limit of a broad range of values reported (1–4.5),[30,31] the most precise determinations coming from cross-linking of low molecular weight PDMS. Again the q_0's found in the literature are for networks produced by γ-irradiation, and the differences relative to the value obtained in this study could be ascribed to different efficiencies of the radiation for the cross-linking process. Also, recent computer simulations of the random cross-linking process of polymer chains[31,33] show that the probability of intramolecular linking is not negligible. They predict that the fraction of the cross-links consumed in intramolecular processes increases with the molecular weight of the chains and that it can account for as much as 30% of the total number of cross-links when these are distributed randomly as is expected to happen in networks produced by high-energy electron irradiation. This may contribute to explain the relatively low q_0 value obtained.

Since the model used to fit the gel weight fraction data does not consider intramolecular linking and main-chain scission is negligible (thus affecting little the gel weight fractions), the q_0 obtained should be considered as an *effective* intermolecular cross-linking density.

3. Equilibrium Swelling Measurements

Information on the network structure was obtained from results of macroscopic equilibrium swelling experiments in which three different solvents were used. The results were interpreted in the framework of the classical phantom network models, and compared with predictions of a statistical approach.

3.1. Introduction. In the classical thermodynamic approach,[1] the change in the Gibbs function of a polymer network upon swelling depends on the change due to mixing of polymer and solvent, ΔG_{mix}, and to the elastic deformation of the network, ΔG_{el}, the two contributions being considered additive:

$$\Delta G = \Delta G_{\text{mix}} + \Delta G_{\text{el}}$$

In terms of the chemical activity a_s of the solvent in the network

$$\ln a_s = \ln a_{s,\text{mix}} + \ln a_{s,\text{el}} = \left[\frac{\partial G_{\text{mix}}}{\partial n_s} + \frac{\partial G_{\text{el}}}{\partial n_s}\right]/kT \quad (7)$$

where n_s is the number of solvent molecules in the system.

The mixture term is evaluated in the framework of the Flory–Huggins lattice model for polymer solutions:[1]

$$\ln a_{s,\text{mix}} = \ln(1-\phi_p) + \phi_p(1-x) + \chi\phi_p^2 \quad (8)$$

where ϕ_p is the polymer volume fraction, x represents the ratio between the average number of segments in a polymer molecule to that in a solvent molecule ($1/x \sim 0$ for a network), and χ is the Flory–Huggins polymer–solvent interaction parameter. The elastic contribution to the chemical activity of the solvent is calculated using

$$\ln a_{s,\text{el}} = \left(\frac{\partial G_{\text{el}}}{\partial n_s}\right)/kT = \left(\frac{\partial G_{\text{el}}}{\partial \lambda}\right)\left(\frac{\partial \lambda}{\partial n_s}\right)/kT \quad (9)$$

where λ is the linear extension ratio ($\lambda^3 = Q = V/V_0$). At equilibrium swelling, the elastic and mixing contributions must cancel.

The classical reference models to calculate the elastic contribution are the *phantom*[5] and *affine*[4] network models. They both derive the elastic contribution under the assumptions that the strands in between junctions (cross-links) are dimensionless and that their conformation obeys Gaussian statistics.

In the affine model, the junctions are assumed to be firmly embedded in the network, their relative positions being determined by the macroscopic deformation. The change in elastic contribution for an isotropic deformation is

$$\Delta G_{\text{el}}^{\text{aff}} = 3kT[{}^1/_2\nu(\lambda^2 - 1) - \ln \mu] \quad (10)$$

where ν and μ are, respectively, the number of elastically effective strands and junctions.

In the phantom network model the junctions are assumed to fluctuate around mean positions that are determined by the macroscopic deformation. In this case the elastic contribution can be written

$$\Delta G_{\text{el}}^{\text{ph}} = {}^3/_2 kT\xi(\lambda^2 - 1) \quad (11)$$

where ξ is the network cycle rank (the number of cuts

required to reduce the network to an acyclic tree). For a perfect network

$$\xi = \nu - \mu \tag{12}$$

$$\mu/\xi = 2/(f-2) \tag{13}$$

where f is the junction functionality, i.e., the number of elastically effective strands emanating from a junction. For tetrafunctional junctions $\xi = \mu = \nu/2$.

Expressed in terms of cycle density, $\xi^* = \xi/V_0$, where V_0 is the network volume in the state of preparation, the equilibrium swelling conditions can be expressed for both models as

$$\xi^* = -F\frac{\ln(1-\phi_p) + \phi_p + \chi\phi_p^2}{V_s(\phi_p/\phi_{p0})^{1/3}} \tag{14}$$

where V_s is the molar volume of the solvent, ϕ_{p0} is the polymer volume fraction in the state of preparation, and F is a factor whose value is 1 in the case of the phantom model and

$$F_{aff} = \frac{1}{1 + 2[1-(\phi_p/\phi_{p0})^{2/3}]/(f-2)} \tag{15}$$

for the affine network model.

In terms of the average molecular weight in between links, M_C, eq 14 gives for the phantom model for tetrafunctional links

$$M_C^{ph} = -\frac{1}{2}\rho V_s(\phi_p/\phi_{p0})^{1/3}[\ln(1-\phi_p) + \phi_p + \chi\phi_p^2]^{-1} \tag{16}$$

where ρ is the polymer density. For the affine model, eqs 14 and 15 give

$$M_C^{aff} = [2-(\phi_p/\phi_{p0})^{2/3}]M_C^{ph} \tag{17}$$

The results obtained when using eqs 16 and 17 to interpret the experimental data have to be analyzed with some criticism. In both models it is assumed that the network is ideal, i.e., free of defects such as dangling ends, loops, and local cross-link inhomogeneities. Defects will, however, be present and are expected to be important in network swelling studies because elastically inefective material will not contribute to the elastic behavior, whereas it will contribute to the mixing term. Also the models do not account for the presence of topological entanglements that also contribute to the elastic response. In fact, although an *a priori* knowledge of the network structure is at present still not possible, it is reported that neither of these models gives a good quantitative account of the deformation process.[34-36]

A further problem in the use of eqs 16 and 17 comes from the difficulty in finding in the literature values for the interaction parameter covering the polymer concentration ranges usually present in the swollen networks. It must be stressed that structural parameters obtained using eqs 16 and 17 are particularly sensitive to χ values in the vicinity of 0.5, a value possible to find for most solvent–polymer systems at some polymer concentration.

To overcome the difficulties arising from the chemical interaction between polymer and solvent, three different solvents were used in the swelling measurements. It is expected that a correct description of the elastic contribution produces the same values of M_C independently of the solvent used.

The results obtained were further compared with predictions of a statistical approach that takes into account the molecular weight distribution in the polymer melt.

3.2. Experimental Procedures and Results. Pieces of rectangular shape were cut from each of the samples irradiated with a dose higher than 10 Mrad. Their area was typically 5 × 2 cm² and their thickness around 0.5 mm. Some thicker samples (up to 3 mm) were also used for the sake of comparison. The samples were weighed and their sizes measured before being immersed in an excess of three different solvents (*p*-xylene, toluene, and cyclohexane). For each solvent and each dose, at least two samples were used in the equilibrium swelling measurements except in the case of the samples irradiated to 5.9, 7.1, and 8.1 Mrad, which did not have a well-defined shape. These were only swollen in toluene, and for each of these three doses, only one sample was used.

The networks swollen in *p*-xylene were kept in their bath for 2 days and then remeasured and weighed. The samples swollen in toluene and cyclohexane were kept in the bath close to 3 months. The solvent was periodically renewed and the samples' dimensions were measured.

The equilibrium swelling volume ratio (Q) was calculated as

$$Q = \frac{V_S}{V_0} = \frac{\text{volume of the swollen network}}{\text{volume of the dry network}} \tag{18}$$

for all the samples that had a well-defined shape. For the three lower cross-linked networks it was calculated using

$$Q = (G-1)\frac{\rho_p}{\rho_s} + 1 \tag{19}$$

where G is the ratio between the masses of the swollen and dry networks, and ρ_p and ρ_s are respectively the polymer and solvent densities.

During the swelling process, extraction inevitably takes place. It comes from removal of material not incorporated in the macroscopic cluster. Because the removal of material affects the value of the polymer volume fraction in the swollen network, ϕ_p, the swollen samples were dried and remeasured. The amount of material removed in the swelling bath was estimated by

$$\frac{V_P}{V_0} = \frac{\text{volume of dried polymer after swelling}}{\text{volume of dry polymer prior to swelling}} \tag{20}$$

Calculating the ratios

$$\omega = \frac{V_P}{V_0}\Big/\frac{V_S}{V_0} = \frac{V_P}{V_S} \tag{21}$$

after different times in the washing bath, ω values ranging from slightly less than 1 after 1 h (almost no extraction to $\omega = \omega_g$ after 1 month (complete extraction) were found. The rate of change in ω depends on both irradiation dose and sample thickness. However, there was no detectable change in the volume of the swollen samples after the first few hours in the bath (less than 1 h for the higher linked ones and less than 6 h for the one irradiated to 10 Mrad). This suggests that the network expansion is not significantly influenced by the presence of the soluble components in the early stages of solvent absorption. After the equilibrium volume is reached, the volume occupied by the soluble part is, with time, essentially replaced by solvent.

The equilibrium swelling ratios in xylene are shown as a function of received dose in a double-logarithmic plot in Figure 3a. For doses higher than 11 Mrad, the swelling ratios fall on a straight line. A linear fit to the experimental points (also shown in Figure 3a) gives a slope -0.59 ± 0.02, implying the approximate scaling relation

$$Q \sim r^{-3/5} \tag{22}$$

in agreement with other studies on cross-linked sili-

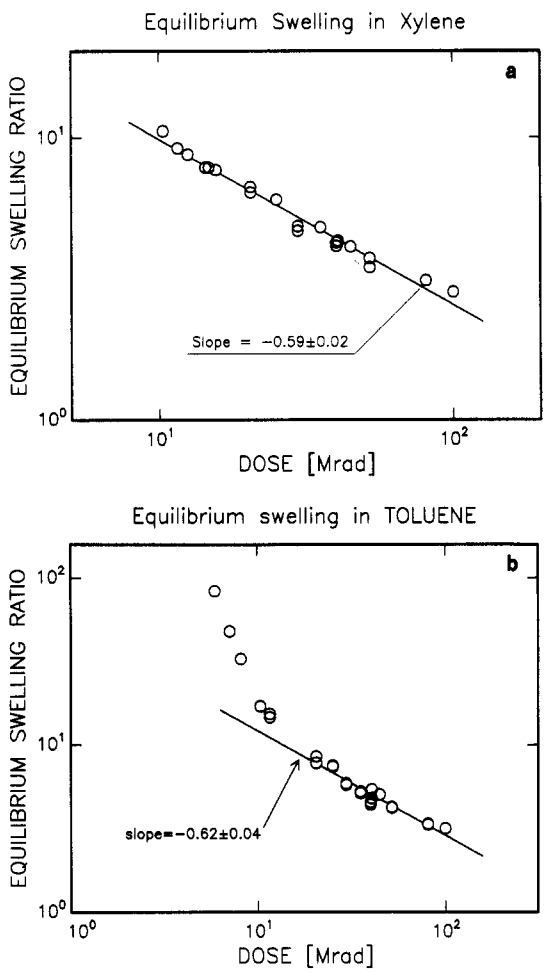

Figure 3. Double-logarithmic plot of the equilibrium swelling ratios $Q = V/V_0$ as a function of irradiation dose. (a) Swelling in xylene. The full line is the result of a linear fit to the experimental points obtained from samples irradiated to $r > 11$ Mrad. (b) Swelling in toluene. For doses higher than ~11 Mrad the experimental points fall on a straight line. Approaching the gel point, the Q values diverge to a much higher power law dependence on the irradiation dose.

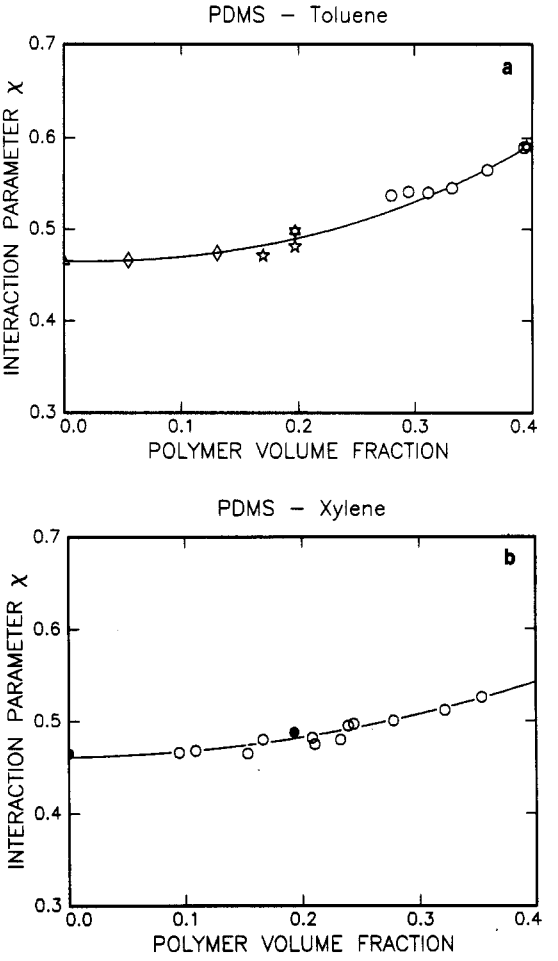

Figure 4. (a) Dependence of the Flory interaction parameter χ on polymer volume fraction ϕ for the system PDMS–toluene. The points were obtained from the literature, and the full line is a polynomial fit to the points. (b) Interaction parameter χ for the system PDMS–xylene. The points are calculated from average N_C values obtained from swelling in toluene and cyclohexane using eq 16 (open circles) and reported values (filled circles). The full line is the result of a fourth-order polynomial fit to the experimental values.

cones.[37,38] However, closer to the gel point, as seen from the swelling in toluene (Figure 3b), the swelling ratio deviates clearly from this behavior, diverging to much higher values. In this solvent, once again, the scaling relation $Q \sim r^{-3/5}$ is found for samples irradiated to doses sufficiently far away from the gelling dose. A linear fit to the experimental points obtained from the samples irradiated to doses higher than 11 Mrad gave a slope −0.62 ± 0.04.

3.3. Phantom Network Models. For the systems PDMS–toluene and PDMS–cyclohexane, χ values covering the polymer volume fractions present in the swollen networks are available in the literature. A fourth-order polynomial, obtained from fitting published values,[39,41–43] was used to describe the dependence of χ on polymer volume fraction for the system PDMS–toluene (Figure 4a). The following result was obtained:

$$\chi_{tol} = 0.4652 - 0.02797\phi_p + 0.777\phi_p^2 - 0.26682\phi_p^3 + 1.2990\phi_p^4 \quad (23)$$

For the system PDMS–cyclohexane a linear polynomial was used to describe the data:

$$\chi_{cyc} = 0.4280 + 0.08999\phi_p \quad (24)$$

The number of monomers in between elastically effective links $N_C = M_C/m_0$ was calculated from eqs 16 and 17. A good agreement between the results from swelling in toluene and cyclohexane was obtained within the affine network model for the networks produced at intermediate and high irradiation doses. The N_C values obtained are shown in Figure 5. For ($r \geq 12$ Mrad) the N_C values obtained for the swelling in toluene and cyclohexane agree within 10%. For the low irradiation dose networks, the differences are more important. The results were checked by calculating the χ concentration dependence for the system PDMS–xylene. For each sample the average N_C taken from swelling in toluene and cyclohexane was used in eq 16 to calculate χ. The values found were fitted to fourth-order polynomials and compared with some values reported[39,40] (Figure 4b). The agreement is quite good.

For the samples irradiated to $r \geq 11$ Mrad, the dependence of $\log(N_C)$ on $\log(r)$ is closely linear. A straight line fitted to the experimental points, also shown in Figure 5, produced the slope −1.53 ± 0.06. The results of the fit indicate that the number of monomers in between elastically effective links decreases with irradiation dose according to a scaling relation:

$$N_C \sim r^{-3/2} \quad (25)$$

Combining this power law with the dependence on dose of the equilibrium swelling ratio (eq 22), the following relation between the polymer volume fraction in the

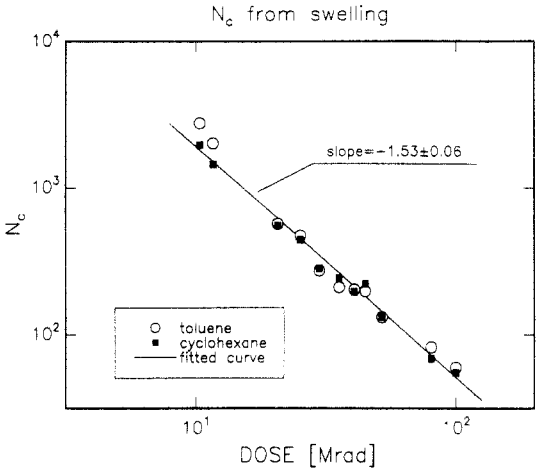

Figure 5. Double-logarithmic plot of the average number of monomers in elastically effective network strands N_C as a function of the irradiation dose. The values were obtained from equilibrium swelling in two different solvents, toluene (open circles) and cyclohexane (filled boxes), using the phantom network model. The full line is the result of a linear fit to the experimental points.

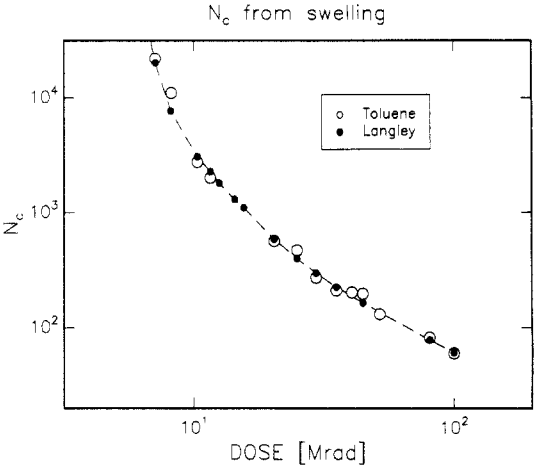

Figure 6. Comparison between the N_C values obtained with the phantom network model from equilibrium swelling in toluene and calculated values using eq 27 by adjusting the number of entanglements in the melt to 10 mol/m^3.

swollen network and the average number of monomers per elastically effective strand is found:

$$\phi_p \sim Q^{-1} \sim [(N_C^{-2/3})^{-3/5}]^{-1} \sim N_C^{-2/5} \qquad (26)$$

This result is a consequence of the N_C dependence on dose and deviates from the $-3/5$ dependence usually quoted that results from the development in power series of the logarithm present in the mixing contribution and the assumption of a constant χ value.

3.4. Statistical Approach. Further information on the network structure was obtained from a statistical approach which gives results that are independent of the chemical interaction between polymer and solvent. Elastically effective strand densities were evaluated using expressions that also account for the presence of defect structures[26] (namely dangling ends and trapped entanglements). Following Scanlan's method[44] that counts one effective strand between cross-links if both of them are connected to the gel by three or more paths, the number of monomers in between elastically effective links is written[26]

$$N_C^{-1} = \frac{q}{2}[3\omega_g T_e^{1/2} - T_e/2] + \epsilon T_e \frac{m_0}{\rho} \qquad (27)$$

with T_e (the fraction of original entanglements in the melt that become trapped in the network production process) given by

$$T_e = x^4[1 - 2(1 - \sum_{P=1}^{\infty} N_P e^{-yP})/y\bar{P}_n + 1/\bar{P}_n \sum_{P=1}^{\infty} N_P e^{-yP}]^2 \qquad (28)$$

In this expression ϵ is a factor that accounts for the effective entanglement density in the melt. The other quantities have been introduced in connection with eqs 4, 5, and 6.

Using the GPC results for the molecular weight distribution in the melt and adjusting the parameter ϵ to 10 mol/m^3, a remarkably good agreement with the N_C's from the equilibrium swelling measurements was obtained (particularly for intermediate and highly cross-linked samples). The results are plotted in Figure 6 together with the values obtained from equilibrium swelling in toluene. The ratio, $r_{\nu e}$, between the density of network strands ν_s and the density of dangling ends ν_e was calculated using

Table II. Ratio, $r_{\nu e}$, between the Density of Network Strands ν_s and the Density of Dangling Ends ν_e Calculated Using Equation 29

dose (Mrad)	ν_s/ν_e	dose (Mrad)	ν_s/ν_e
4.76	0.001	15.65	0.734
5.93	0.020	20.49	1.122
7.11	0.086	25.09	1.443
8.15	0.178	29.66	1.718
10.35	0.353	35.41	2.030
11.61	0.439	44.72	2.426
12.57	0.519	80.61	3.615
14.41	0.652	99.98	4.125

$$\tau_{\nu e} = \nu_s/\nu_e = \left[\left(\frac{q\rho}{m_0}\right)[3\omega_g T_e^{1/2} - T_e/2] + 2\epsilon T_e\right] \Big/ \left[2\rho x\left\{M_n^{-1}(1 - \sum_{P=1}^{\infty} N_P e^{-yP}) + pm_0^{-1}\left[\frac{1 - (1 - \sum_{P=1}^{\infty} N_P e^{-yP})}{y\bar{P}_n}\right]\right\}\right] \qquad (29)$$

The results are presented in Table II.

For the samples irradiated to doses higher than 12 Mrad, the agreement between the two independent ways of calculating the molecular weight in between elastically effective links is quite good. It should be noted that the value $\epsilon = 10$ mol/m^3 needed to adjust to the data is quite reasonable for this PDMS melt. It corresponds to an entanglement distance of ~55 Å, a value within the range 40–70 Å reported[45,46] from measurements of the plateau modulus for the tube diameter of PDMS (roughly associated with the average entanglement distance).

Below 12 Mrad, the differences in the results coming from the different approaches and the swelling in different solvents are clear. They could be attributed to inaccurate values of the interaction parameter but, more likely, the differences observed are related to the number of dangling ends present at low cross-link densities. As seen from Table II, the number of chains connected to the macroscopic network by a single link is extremely high at low

dose. Only when $r_{\gamma_e} = 0.5$ does each chain have, on average, two linked monomers, and for our networks this happens at irradiation doses around 12 Mrad.

Summarizing the results obtained from the equilibrium swelling measurements and from the theoretical statistical approach to the cross-linking process, it is possible to say that, while the numerical values may be incorrect on an absolute scale (there is no independent way of confirming them), at least they are mutually in good agreement, and, in particular, they both show the same scaling behavior of the elastically effective strand mass with irradiation dose.

Under the assumption that the statistical approach provides a good description of the effect of the irradiation on the network structure, the results indicate that the classical *phantom network models* describe qualitatively the macroscopic swelling of the highly irradiated samples.

4. Small-Angle Neutron Scattering

The microscopic structure of the networks was studied by performing small-angle neutron scattering (SANS) measurements in networks swollen to equilibrium. The measurements were done at the SANS instrument installed at the DR3 reactor of the Risø National Laboratory. Labeling techniques make SANS a particularly powerful method to access the microscopic structure of polymeric systems. Using fully deuterated solvent, a good contrast between polymer and solvent is established, and the scattered intensity gives information on the correlations between all monomers.

Because the scattering patterns recorded from the swollen networks showed, in the high scattering vector q region, clear similarities with those typical of polymer solutions, also polymer solutions in the same deuterated solvent were measured. For both solutions and swollen networks, the solvent used was fully deuterated *p*-xylene. In the following, the results obtained for the solutions will be presented first, in order to be used in the discussion of the scattering from the swollen networks.

4.1. Experimental Procedures. The polymer concentrations in the solutions measured, expressed in mg/mL, were 1.77, 4.54, 9.47, 14.77, 25.69, 33.72, 59.21, 90.00, 120.32, 158.76, 228.69, and 318.81. The solutions were mounted in quartz cuvettes with a 1-mm flight path.

To collect the scattered intensity over a broad q range with reasonable instrumental resolution, each sample was measured using several different instrumental settings (neutron wavelength and sample–detector distance). The reciprocal space region explored in this way ranged from 0.003 to 0.1 Å^{-1} for the samples with polymer concentations 1.77, 4.54, 9.47, and 25.69 mg/mL and 0.003–0.45 Å^{-1} for all the others. All measurements were performed at room temperature.

For the networks the scattered intensity was recorded from samples cross-linked at 12 different irradiation doses: 8.1, 10.4, 11.6, 12.6, 14.4, 15.1, 25.0, 35.4, 40.6, 44.8, 80.6, and 99.9 Mrad.

For irradiation doses higher than 10.4 Mrad, the cross-linked samples measured had rectangular shape and thicknesses ranging from 0.1 to 0.5 mm. The sample cross-linked with 8.1 Mrad had a very irregular shape due to difficulty in manipulation. The one cross-linked with 10.4 Mrad was made out of small pieces cut from a thicker sample.

Prior to the measurements, they were placed inside the quartz cuvettes where they were measured and immersed in an excess of fully deuterated *p*-xylene. They were then allowed to rest for times that ranged from 12 h to 1 day, to reach the equilibrium swelling degree. The soluble part was not removed from the cuvettes.

For irradiation doses above 10.4 Mrad, the samples keep their rectangular shape upon swelling. Their thicknesses in the swollen state were estimated using the equilibrium swelling ratio curve obtained with the protonated solvent. For the two lower dose samples the estimated thicknesses are not precise due to their irregular shape.

As for the semidilute solutions, each sample was measured using several different settings of the spectrometer. The reciprocal space region explored ranged from 0.0033 to 0.45 Å^{-1}. These measurements were also performed at room temperature.

Subtracted from the two-dimensioinal raw data was the background coming from the quartz cuvette, from the deuterated solvent, and from other sources to the experimental background that were accounted for by replacing the sample by a neutron absorber (B_4C). The incoherent signal of a 1-mm-thick water sample was used to correct for variations in detector efficiency and to have the data on an absolute scale. Since the scattering patterns have azimuthal symmetry, the data were reduced to the one-dimensional intensity $I(q)$ that only depends on the absolute value of the scattering vector. The scattering spectra analysis was performed by a least-squares fitting program that includes the instrumental smearing effects using a resolution function and fits simultaneously the data recorded with the different spectrometer settings.[47] The incoherent background was included as a constant in the fitting function.

4.2. Polymer Solutions. 4.2.1. Introduction. At high degrees of dilution, when the polymer coils are well separated from each other (*dilute solutions*), the scattering intensity is the result of the incoherent sum of the intensities scattered by each coil. For small values of the scattering vector q ($qR_G < 1$, where R_G is the gyration radius of the coils), the shape of scattering curve is sensitive to the average values of the polymer chain mass (the average molecular weight M_w) and size (given by the radius of gyration R_G). For values of the scattering vector q such that $qR_G > 1$, the scattering probes the local conformation inside the coil. In a good solvent the intrachain correlations obey excluded volume statistics (the mass distribution inside the coils is fractal, $M \sim R^{D_F}$, with $D_F = 5/3$ for good solvents). For $qR_G > 1$ the scattering intensity is thus $I(q) \sim q^{-D_F}$. Changing the polymer concentration in the *dilute* regime results in changing the number of coils exposed to the beam, and consequently the intensity scattered simply scales with the polymer concentration.

Increasing the polymer concentration above a certain characteristic concentration c^* at which the coils are in contact, the polymer chains will interpenetrate. Polymer solutions with concentrations such that $c > c^*$ but still $c \ll 1$ are said to be *semidilute*. The transition between the dilute and semidilute concentration regimes is not sharp but extends over a certain range of c values around c^*. In the *blob* picture,[48] a semidilute polymer solution in a good solvent has a characteristic length ξ, the correlation length of the concentration fluctuations. For distances $r < \xi$, the mass distribution in the system obeys the fractal law of a *self-avoiding walk* ($m \sim \xi^{5/3}$). For distances $r > \xi$, the semidilute solution looks like a closed-packed system of blobs. The concentration fluctuations are correlated inside each blob but uncorrelated with respect to any other blob. For $q\xi > 1$ the scattering intensity is $I(q) \sim q^{-5/3}$. And

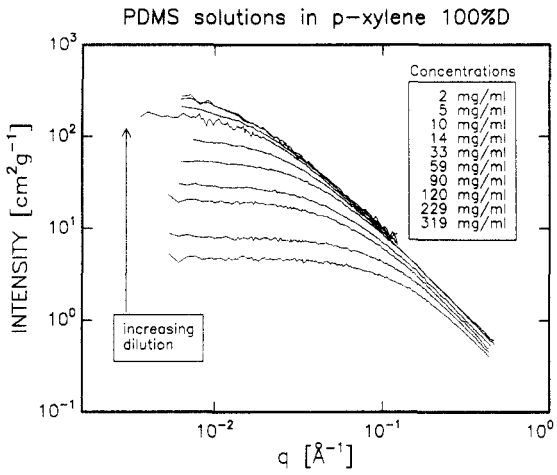

Figure 7. Small-angle neutron scattering from PDMS solutions in fully deuterated *p*-xylene. Double-logarithmic plot of the coherent scattered intensity normalized by concentration as a function of scattering vector q.

for $q\xi < 1$ it obeys the Lorentzian scattering law:[48]

$$I(q) \simeq c^2\xi^3/(1 + q^2\xi^2) \tag{30}$$

The average polymer concentration, valid for all scales greater than ξ, is $c \sim m/\xi^3 \sim \xi^{5/3-3}$, giving $\xi \sim c^{-3/4}$. So, increasing the system dilution in the *semidilute regime* results in an increase in the blob size (small blobs rearrange through disinterpenetration in less numerous larger blobs). With increasing dilution, the intensity in the limit of zero scattering vector increases: $I(q=0) \sim c^2\xi^3 \sim c\xi^{D_F}$, which with $D_F = {}^5/_3$ gives $I(q=0) \sim c^{-1/4}$.

4.2.2. Results and Discussion. Figure 7 shows, normalized by concentration, the spectra obtained for most of the concentrations measured. As seen from the figure, for intermediate values of the scattering vector the power law dependence characteristic of the fractal self-avoiding walk of the chains is clearly present as is the shift of the correlation length to higher values with increasing dilution.

The correlation length ξ_S was obtained by fitting the spectra using the Lorentzian eq 30 in the region where $q\xi_S < 1$. The concentration dependence of the correlation length is shown in a log–log plot in Figure 8a. From the plot it is evident that the set of concentrations measured cover the crossover from the dilute to the semidilute concentration regimes. With increasing polymer concentration, the correlation length goes from an almost constant, c-independent value, characteristic of dilute solutions, for which the ξ_S values should rather be considered as apparent correlation lengths, whose limiting value at $c \to 0$ is

$$\xi_{app} \to R_G/3^{1/2} \tag{31}$$

to a power law dependence on c that is characteristic of the semidilute regime. The presence of the transition between the two concentration regimes is also evident in Figure 8b, where the scattered intensities in the limit of zero scattering vector are shown as a function of concentration in a log–log plot. Increasing c, $I(0)$ first increases proportionally to concentration (dilute regime) and after a certain concentration it decreases until reaching a powerful law dependence on c. Linear fits to the points corresponding to the five higher concentrations measured gave the following relations:

$$\xi_S \sim c^{-0.75\pm0.02} \tag{32}$$

$$I(q=0) \sim c^{-0.50\pm0.03} \tag{33}$$

The ξ_S dependence on c is exactly the $-{}^3/_4$ predicted by

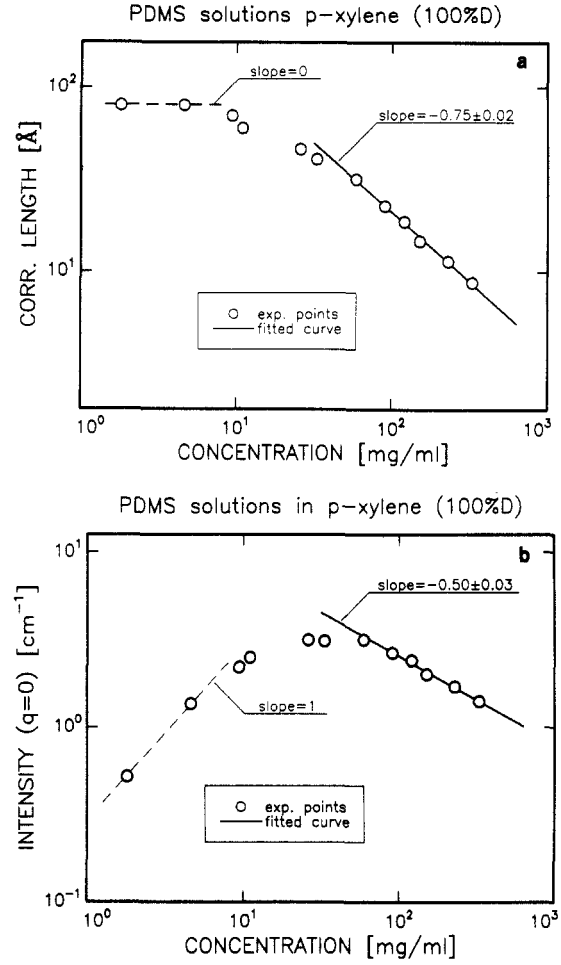

Figure 8. (a) Correlation length ξ_S as a function of polymer concentration. The open circles are the values obtained from fitting a Lorentzian scattering function to the low scattering vector part of the experimental spectra. The full line is a linear fit to the higher five polymer concentrations measured. The broken line has a slope of zero. (b) Intensity scattered in the limit of zero scattering vector. The open circles are the values obtained from the Lorentzian scattering function. The full line is a linear fit to the higher five polymer concentrations measured. The broken line has a slope of 1. The symbol size is of the order of the larger error bar.

scaling theories for semidilute solutions in good solvents. It is remarkable that the semidilute description holds here up to concentrations as high as 319 mg/mL, for which the polymer volume fraction is $\sim {}^1/_3$, but this was also observed in polystyrene solutions in toluene.[50,52]

The exponent found for the dependence of $I(q=0)$ on polymer concentration deviates from the power $(-{}^1/_4)$ expected from scaling theories. It is, however, in good agreement with the value 0.45 ± 0.05 reported[49] for PDMS solutions in toluene. The higher power law found seems to suggest that the blobs contain more mass than what would be expected from the scaling argument. A tentative explanation for the effect would be to attribute it to the presence of the small molecular weight chains. These are expected to act as solvent for the longer chains[48] if their number of monomers is lower than the square root of the number-average number of monomers in the sample. This aspect was not investigated further.

In the dilute regime and the limit of zero concentration, we find that ξ_S approaches a value $\simeq 73$ Å. The dilute solutions were also fitted in the low-q region using the Zimm relation:

$$Kc/S(q) = M^{-1}(1 + q^2R_G^2) + 2A_2c + O(c^2) \tag{34}$$

An extrapolation to the zero concentration limit gives the

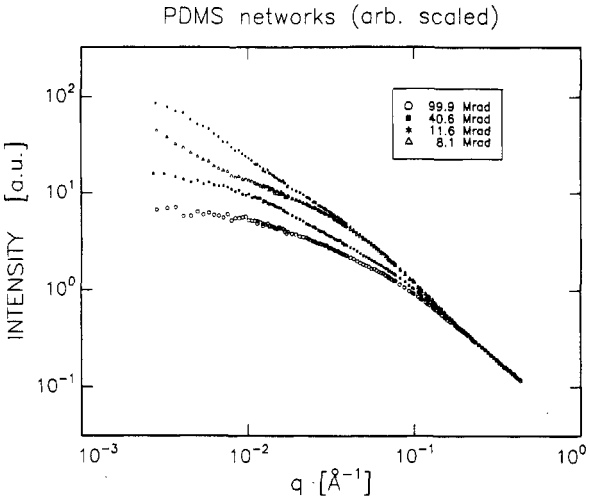

Figure 9. Small-angle neutron scattering from PDMS networks swollen to equilibrium in fully deuterated *p*-xylene. Double-logarithmic plot of the total scattered intensity as a function of scattering vector q for four of the samples measured. The experimental spectra are arbitrarily scaled to the 11.6-Mrad spectrum to better display the differences in scattering profile.

molecular weight $M_w \simeq 62\,500$, a value that is ~18% off the one obtained from the GPC molecular weight distribution, and a gyration radius $R_G \simeq 125$ Å, in good agreement with the value 127 Å obtained from eq 31.

4.3. Networks Swollen to Equilibrium. 4.3.1. Introduction. Figure 9 shows, in a double-logarithmic plot, curves of the total intensity scattered from samples with different cross-link densities. To make the differences in shape more evident, the spectra in Figure 9 are arbitrarily scaled to the 11.6-Mrad sample spectrum in such a way that they overlap in the high-q region. At high q the shape of the signal is always close to the one obtained from polymer semidilute solutions (Figure 10a, where the signal obtained from the swollen 10-Mrad sample and the one from the equivalent solution are shown, gives a clear example of this). However, at low q there is an increase in the signal produced by the networks relative to what is observed in semidilute solutions. This is found for all network samples measured. The q value at which the signal from the gel deviates from the *solution-like* profile increases with increasing dose. At intermediate and low scattering vector the shape of the scattering curves is very much dependent on cross-link density. Focusing on the scattering spectrum recorded for the sample irradiated to 40.6 Mrad, which displays typical features present in the other spectra, one sees that it is possible to identify three main regions in the double-logarithmic plot: At high q the shape of the signal is always *solution-like* (with a final slope $-5/3$); at intermediate q vector the scattering curve also obeys a $I \sim q^{\alpha}$ relationship but with an exponent α different from the limiting high-q one; at low scattering vector there is a crossover to a q region where the signal becomes q independent. The transition between the different linear behaviors at high and intermediate q is clear and, in this case, narrow. For the low cross-linked samples, this transition is more extended (8.1-Mrad sample in Figure 9) and has exactly the shape of the crossover present in a semidilute solution. The effect of increasing irradiation dose in the high scattering vector *solution-like* crossover at high q is to make it less and less pronounced. For the samples irradiated to the higher doses (80.6 and 99.8 Mrad) it is hardly detectable. On the other hand, the low-q crossover, which is not seen in the low cross-linked samples, becomes more and more evident with increasing dose, shifting in position to higher scattering vector values. We attribute the excess scattering at low q to be due to the presence of large-scale heterogeneities. With increasing dose, their spatial extent is reduced.

The large-scale heterogeneities revealed in these experiments are characteristic of randomly cross-linked gels. In particular, they were also observed in PDMS networks that were produced by using a chemical cross-linker and later swollen in toluene.[50,51] They are not expected from the perfect network expansion assumed in the classical models, and these have been unsuccessful in explaining the scattering pattern of gels.[19,21,22]

The analysis of the experimental data performed in the present work was inspired by a recent model[23] that explains, at least qualitatively, some general features of the intensity scattered by gels. Its general assumptions and predictions will be briefly reviewed.

The model was suggested by results, similar to those reported here, obtained from scattering measurements performed on polystyrene (PS) networks produced by cross-linking PS semidilute solutions. Picturing the system in the preparation state as a melt of blobs, it introduces the so-called *frozen blob*, a segment that results from junctions produced on near neighbor sites and that cannot be expanded or stretched upon swelling since in the preparation bath they are supposed to be already in an ideal excluded volume conformation. The network formation is viewed as resulting from the process of randomly linking blobs. With increasing cross-link density, clusters of frozen blobs will be created and at a certain cross-link density (higher than that corresponding to the gel point for the network) the frozen blobs percolate through the system. The frozen blob clusters are assumed to have the shape of percolation clusters: very polydisperse, highly interpenetrated, the large ones being self-similar. The swelling of the system is described by the dilution of these clusters, with the small clusters being partially expelled by the large ones. From an analogy with a random walk of branched macromolecules, the model predicts that (i) the typical size of the large clusters, ξ_{gel}, scales with polymer volume fraction as $\xi_{gel} \sim \phi^{-5/3}$, (ii) the intensity scattered for $q\xi_{gel} > 1$ is $I(q)_{q\xi_{gel}>1} \sim q^{-8/5}$, (iii) $I(q=0) \sim \phi^{-5/3}$, and (iv) a maximum in $I(q=0)$ must occur at a certain cross-link density (corresponding to the blob percolation threshold).

4.3.2. The Model. Our networks are prepared by cross-linking the melt, so the semidilute blob is not present in the preparations state and the notion of the frozen blob as a kind of building unit of the random structure cannot be simply imported from the model described above. Nevertheless, as already mentioned, the shape of the scattered signal in the high scattering vector region is so close to the one produced by a semidilute solution with the same concentration that one is led to conclude that, at small length scales (below a certain characteristic length), the monomers in the swollen network arrange in a self-avoiding walk just like in a semidilute solution. But here it would probably be more appropriate to talk about a distribution of blob sizes. Stated in different words, when probed with a gauge larger than the equivalent solution blob size, the system exhibits clear density fluctuations. These can be qualitatively understood as resulting from the random cross-linking process. Significant fluctuations in cross-link density will be present. In contact with the solvent it is reasonable to expect that the solvent will preferably occupy regions where the local cross-link density is lower, because local rearrangements of the network chains will be more difficult in locally higher cross-linked regions. The swollen network will be heterogeneous

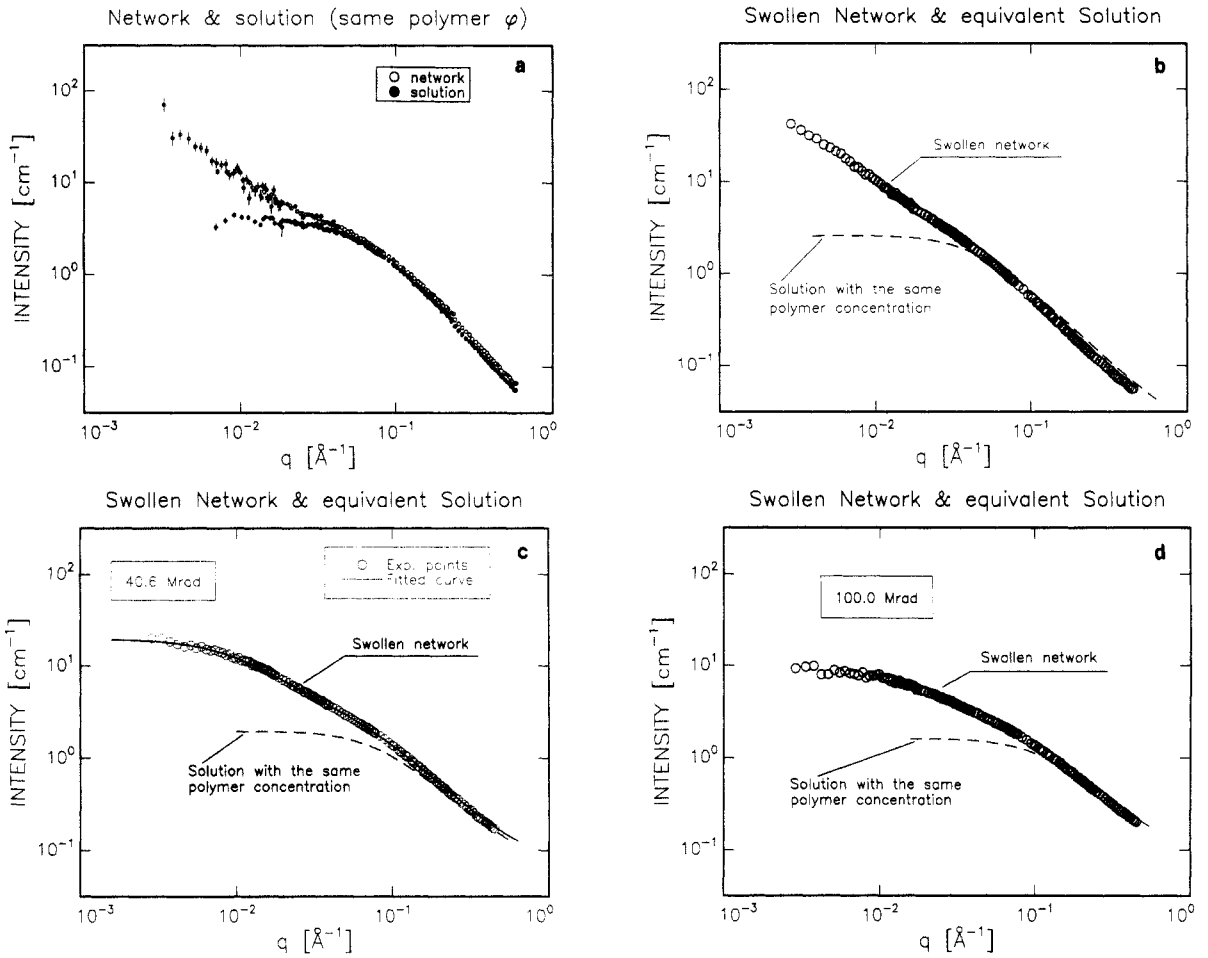

Figure 10. Comparison between the signal obtained from swollen networks and semidilute solutions with the same polymer concentration. In the low scattering vector part the signal from the swollen network deviates clearly from the solution one. (a) Intensity coherently scattered obtained from the network sample irradiated to 10 Mrad (open circles) and from the equivalent solution (filled circles). (b–d) Open circles, total scattering spectra from network samples irradiated to 11.4 (b), 40.6 (c), and 100 Mrad (d). The broken lines are obtained using eq 38 and assuming that the correlation length ξ_S and the intensity $I(q=0)$ depend on polymer concentration as given by eqs 32 and 33.

at larger length scales than a solution with the same polymer concentration, where the chains are completely free to rearrange. Figure 11 gives a schematic representation of a swollen gel (Figure 11b) and the corresponding solution (Figure 11a). At small length scales (inset i), the two are indistinguishable—the mass distribution is fractal and the chain conformation is well described by a self-avoiding walk in both cases. However, at larger length scales (larger than the blob size for the solution) (inset ii), the solution is homogeneous whereas the swollen gel exhibits concentration fluctuations. Only at sufficiently high length scales (inset iii) will these fluctuations not be observed in the swollen gel.

Finally, as seen from the scattering curves (Figure 10), the "average blog size" in the swollen system must be very similar to the ξ_S characteristic of the semidilute solution with the same polymer concentration.

We modeled the large-scale density fluctuations as being fractal, the system beirig pictured as a fractal arrangement of blobs. For the fractal fluctuations the correlation function used was

$$g_{\text{large}}(r) \sim r^{D_L} e^{-r/\xi_L} \tag{35}$$

where D_L is the fractal dimension and the exponential is a cutoff function[53] introduced to account for the finite extent of the fractal correlations. ξ_L is the correlation length that represents the length scale at which the fractal density fluctuations approach the average density in the system.

The scattered intensity can be decomposed in

$$I(q) = \phi_N P(q)\, S(q) \tag{36}$$

where $P(q)$ is the square modulus of the particle form factor $F(q)$ averaged over the ensemble of particles and $S(q)$ is the structure factor describing their spatial distribution. Here the "particle" is associated with the blob characteristic of the semidilute solution with the same polymer concentration.

The fractal contribution to the scattered intensity can be written[54]

$$S_{\text{fractal}}(q) = 1 + \frac{1}{(qr_0)^{D_L}} \frac{D_L \Gamma(D_L - 1)}{[1 + 1/(q\xi_L)^2]^{(D_L-1)/2}} \times \sin[(D_L - 1)\arctan(q\xi_L)] \tag{37}$$

where Γ is the gamma function and r_0 is the gauge of the measurement, which has the characteristic dimension of the individual scatterer. In this expression the first term on the right-hand side (=1) originates from the fact that at a certain scattering vector q the interference between particles is not observed and the scattering is dominated by the particle scattering. For $P(q)$ we built a function that fits the scattering from the solution over all the q range accessed:

$$P(q) \simeq \frac{(1 + q\xi_S)^{1/3}}{1 + q^2\xi_S^2} \tag{38}$$

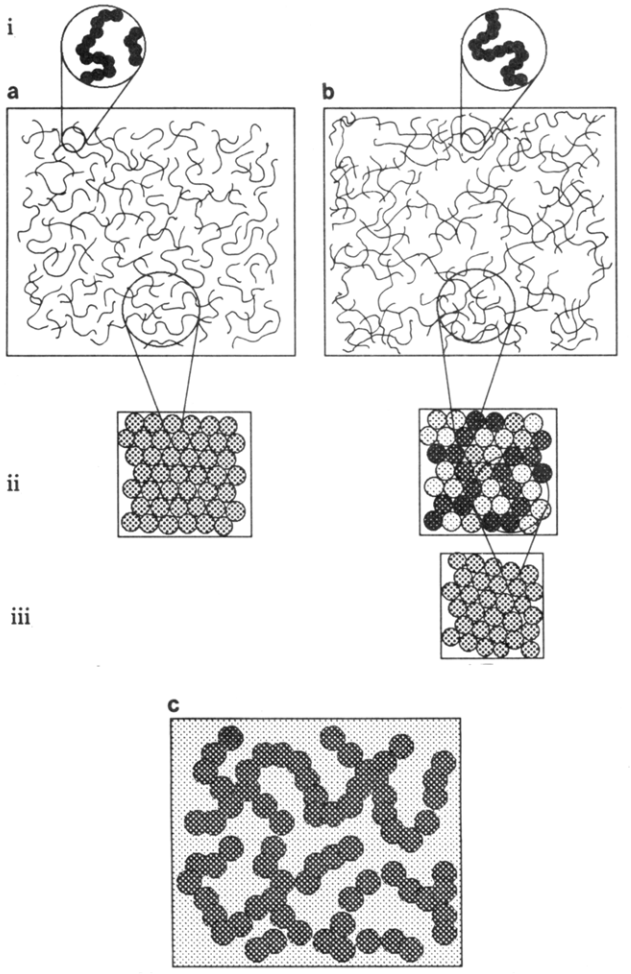

Figure 11. The solution (a) and the network (b) with the same polymer concentration. At small length scales (inset i) the chain is a fractal self-avoiding walk in both systems. At length scales sufficiently above the solution blob size ξ_S (inset ii), the solution is homogeneous. At the same length scale the swollen network displays concentration fluctuations (the solvent occupies preferably regions with locally lower cross-link densities). At some larger length scale (inset iii) the swollen network will also look homogeneous. (c) At large length scales the picture of the swollen network is similar to the one of the equivalent solution at smaller length scales (see text).

The raw data spectra were treated in the way described above for the polymer solutions. All the experimental spectra were analyzed using the scattering function eq 36 even though for the two lowest dose samples the low scattering vector crossover is not present. It was assumed that the length scale above which only the average density is seen was sufficiently large for the corresponding q value not to be accessed in the experiment.

Since the particle is, in the present context, not well defined and the soluble components were not extracted, the experimental spectra were fitted to eq 36 leaving the relative scaling between the self and interference contributions to the scattered intensity as a fitting parameter. The expression used to fit the experimental points was

$$I(q) = A_1 P_{blob}(q) + A_2 P_{blob}(q) \frac{1}{q^{D_L}[1 + 1/(q\xi_L)^2]^{(D_L-1)/2}} \times \frac{D_L \Gamma(D_L - 1)}{\sin[(D_L - 1)\arctan(q\xi)]} + C_{inc} \quad (39)$$

where A_1 and A_2 are scaling factors for the self-correlation and interference contributions to the scattered intensity and C_{inc} is a constant that accounts for the incoherent background. The fitted values of C_{inc} reproduced the incoherent scattering expected from the hydrogen atoms present in the samples.

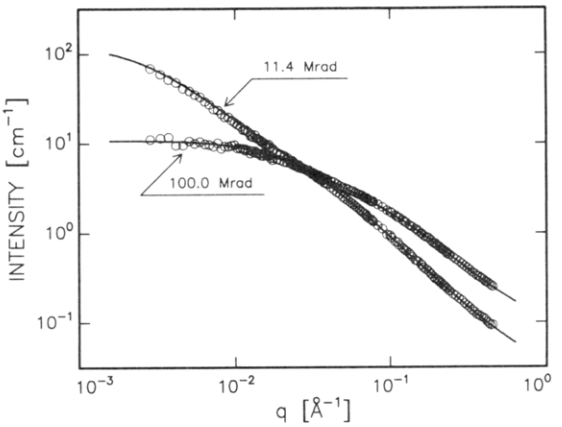

Figure 12. Experimental total scattering spectra and fitted function (full line) as a function of scattering vector q in a double-logarithmic plot for two different networks swollen to equilibrium in fully deuterated p-xylene. The irradiation doses were 11.4 and 100.0 Mrad. The full lines are fitted curves. The symbol size is of the order of the larger error bar.

Table III. Results Obtained from Small-Angle Neutron Scattering Measurements in Networks Swollen to Equilibrium in Fully Deuterated p-Xylene

r (Mrad)	Q	ξ_L (Å)	ξ_S (Å)	ξ_L/ξ_S	$I(q=0)$ (cm^{-1})	scale
8.15	22.0	1758.3	33.2	52.8	360.2	51.0
10.35	12.1	1100.2	29.2	37.9	275.4	49.8
11.60	10.5	400.3	25.5	15.7	69.7	27.6
12.57	8.8	322.1	22.5	14.3	52.5	21.0
14.41	8.0	264.3	20.8	12.7	44.1	17.2
15.10	7.7	218.1	18.3	11.9	32.1	12.3
25.09	5.9	168.2	15.9	10.6	26.6	13.1
35.41	4.8	124.1	14.3	8.6	21.8	9.6
40.57	4.3	108.8	13.0	8.3	19.7	7.6
80.61	3.1	64.3	10.0	6.4	10.8	5.2
99.99	2.8	56.2	9.3	6.0	8.2	4.4

The use of this expression has to be done with some precautions due to the high number of parameters involved. To extract reliable values from the fitting, the number of parameters was first reduced to four by fixing ξ_S to the value of the corresponding semidilute solution. Furthermore, after fitting some of the spectra we realized that, although the shape of the scattering curve is very much dependent on the irradiation dose received, the value of D_L that produced the best fit was within less than 5%, equal to 1.67 ($\sim 5/3$) for all the samples measured. It was therefore fixed to this value, leaving only three parameters to be fitted. After determining the values of the other parameters, the release of the constraints imposed on D_L and ξ_S did not introduce significant changes in their values.

4.3.3. Results and Discussion. Table III summarizes the results for ξ_L, ξ_S, and the "particle" and interference contributions to the intensity scattered in the limit of zero scattering vector, respectively: $I_p(q\to 0) = A_1$ and $I_i(q\to 0) = A_2\Gamma(D_L + 1)\xi_L^{D_L}$ obtained with $D_L = 5/3$. The quality of the fits was excellent for all the samples measured—Figure 12 shows the fitted functions to spectra obtained from two networks with very different cross-link densities.

The intensities I_p and I_i for the samples irradiated to 8.1 and 10.4 Mrad may not be accurate due to the uncertainty in the knowledge of the exact amount of material exposed to the neutron beam. For these samples, also the values of the correlation length of the large-scale density fluctuations are necessarily imprecise because the presence of the crossover is only perceptible by the change

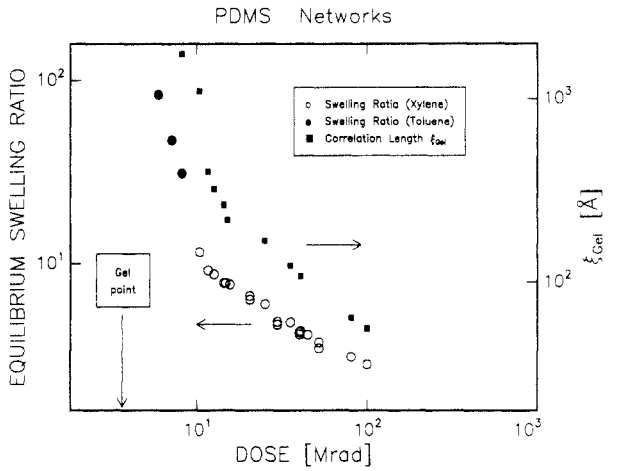

Figure 13. Equilibrium swelling ratio and correlation length for the large-scale concentration fluctuations in the swollen networks as a function of irradiation dose in a double-logarithmic plot.

in slope in the double-logarithmic plot of the scattered intensity versus scattering vector.

The values of ξ_S obtained from the final fits at high q are slightly higher than those of the equivalent solution for all the samples measured as would be expected from the averaging process over a polydisperse ensemble of blobs. The small differences observed suggest, however, that at the scale of ξ_S the fluctuations in concentration are not too important. This is confirmed by the dependence of ξ_S on polymer volume fraction extracted from the double-logarithmic plot of Figure 14a, where the experimental values for the samples cross-linked to doses higher than 11 Mrad are shown. A linear fit to the points gives a slope of -0.75 ± 0.03, so the scaling relation between ξ_S and ϕ_p is, for the swollen networks, exactly $\xi_S{}^g{}_{el} \sim \phi_p{}^{-3/4}$ as in the pure semidilute solution.

The correlation lengths characteristic of the large-scale heterogeneities, ξ_L, are plotted in the double-logarithmic plot of Figure 13 together with the swelling ratios Q as a function of the irradiation dose. The two quantities show a similar dependence on dose and are clearly correlated. As in the case of the swelling ratios, for irradiation doses sufficiently far away from the gel point (for $r > 11$ Mrad), the values of $\log(\xi_L)$ are approximately linearly dependent on $\log(r)$. Approaching the gelling dose, both $\log(\xi_L)$ and $\log(Q)$ diverge in a very similar way.

This divergence in ξ_L and Q can be qualitatively understood in terms of the ratio r_{ν_e} between the densities of elastically effective strands and dangling ends obtained previously from the statistical approach (Table II). Only at an irradiation dose of ~12 Mrad is r_{ν_e} approximately 0.5. Below 12 Mrad and approaching the gelling dose from above, r_{ν_e} decreases very fast, meaning that the network will have a large number of chains bound by a single cross-link and that the number of monomers in between network elastically effective cross-links will be very large. Upon solvent absorption, the loosely bound chains will allow for large-scale rearrangements at the microscopic level, and the density fluctuations are expected to span larger distances. When $r_{\nu_e} \sim 0.5$ the network will start to be well formed (more than two links per chain on the average). With increasing dose, the large-scale rearrangements will be increasingly more difficult. The clear correlation between ξ_L and Q indicates that ξ_L is a microscopic measure of the volume swelling of the network.

A double-logarithmic plot of ξ_L as a function of polymer volume fraction in the swollen networks is shown in Figure 14b. A linear fit to the experimental points gave the slope -1.48 ± 0.04, implying the scaling relation

$$\xi_L \sim \phi_p{}^{-3/2} \tag{40}$$

Equation 40 when combined with the dependence of the average strand mass on dose, eq 25, and the swelling ratio dependence on dose, eq 22, gives

$$\xi_L \sim \phi_p{}^{-3/2} \sim Q^{3/2} \sim r^{-9/10} \sim N_C{}^{-3/5} \tag{41}$$

This relation between the distances spanned by the large-scale density fluctuations obtained from the scattering measurements and the average number of monomers in the elastically effective network strands obtained from the statistical approach is interesting. It is equivalent to state that, in a sphere of radius ξ_L, the number of monomers that contribute to the elastic properties, N_C, obeys a fractal law

$$N_C \sim \xi_L{}^{5/3} \tag{42}$$

with a fractal exponent that is precisely the one that characterizes a fractal self-avoiding walk, suggesting that, over large distances (of the order of the end-to-end distance of the elastically active chains), the swelling of the system can be described by the separation of the network chains, these being organized in some renormalized unit. Note that this would give a simple justification for the fractal dimension $^5/_3$, characteristic of the large-scale density fluctuations, that was found to produce the best fit for *all* the samples measured.

In our model the polymer concentration is considered a continuous variable at sufficiently high length scales, i.e., for distances roughly higher than the solution correlation length (as exemplified in the inset ii of Figure 11b). However, eq 41 seems to suggest that, at the same length scales, the system can be pictured as in Figure 11c where the polymer excess density is *collected* in the dashed regions. Furthermore, at these length scales, the picture of the swollen network must be similar to Figure 11a.

If ξ_L represents the typical distance below which the swollen system can be described as a kind of self-avoiding walk of units of size L, then

$$\xi_L \sim N_L{}^{3/5} L \tag{43}$$

where $N_L = N/g$ is the number of units and g represents the average number of monomers inside the unit. Identifying L with ξ_S and introducing the fact that for distances below ξ_S the monomers conform according to excluded volume statistics ($g \sim \xi_S{}^{5/3}$), eq 41 is recovered. This is also confirmed by the dependence of the ratio between the two characteristic lengths on polymer volume fraction in the swollen network, shown in a double-logarithmic plot in Figure 14c. A linear fit to the experimental points produced the slope -0.73 ± 0.02, implying the approximate scaling relation

$$\xi_L/\xi_S \sim \phi_p{}^{-3/4} \tag{44}$$

The results suggest that, over distances of order ξ_L, the structure of the swollen system can be described as a self-avoiding walk of blobs whose average size ξ_S is roughly equal to the blob size of the equivalent semidilute solution.

From the interpretation given to the two correlation lengths, a maximum in the intensity scattered as a function of cross-link density is not expected at a dose higher than the gelling dose, and it was not observed in the range of irradiation doses accessed. Figure 14c displays a double-logarithmic plot of $I(q=0)$ versus polymer volume fraction

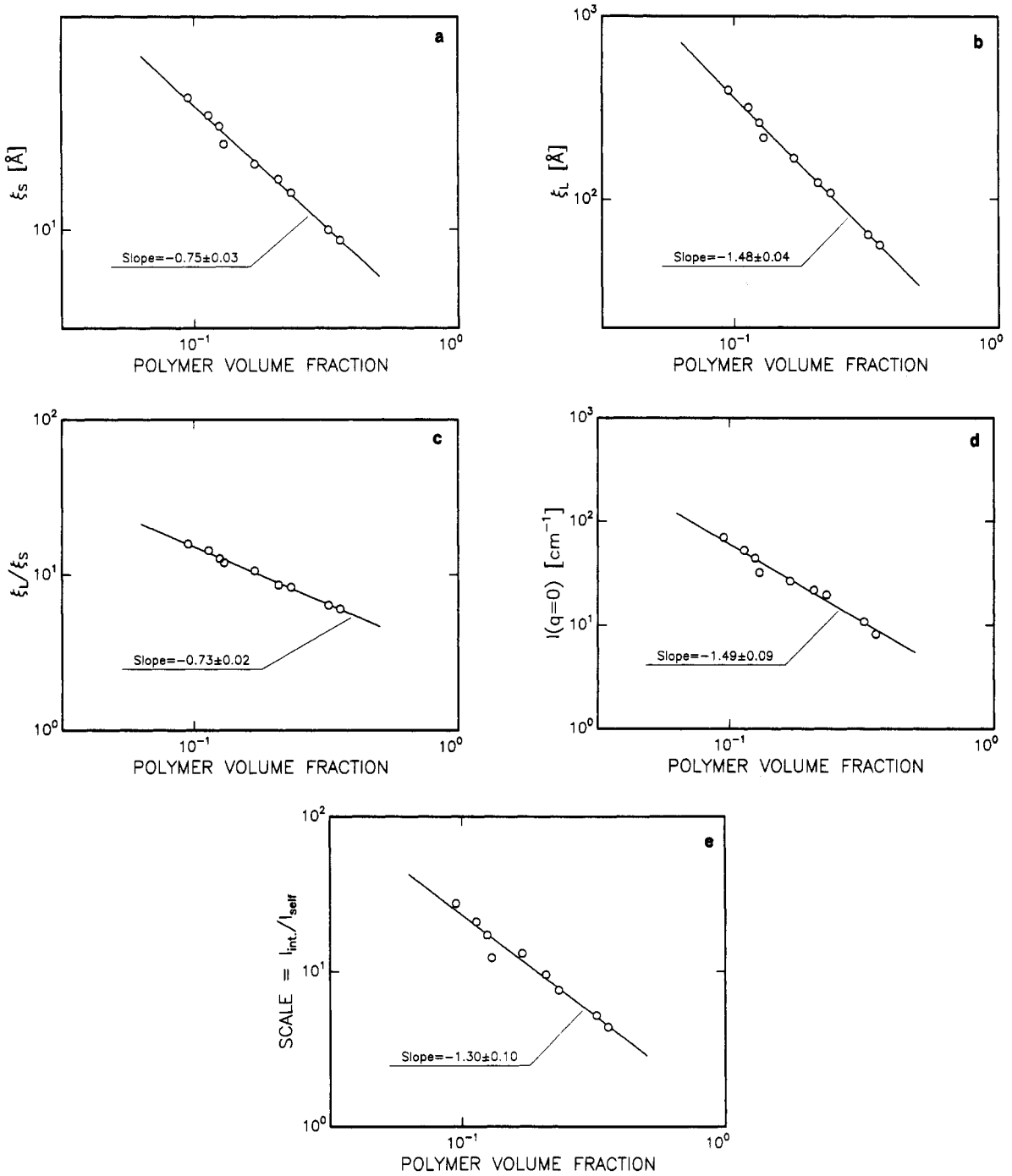

Figure 14. Double-logarithmic plots representing dependences on polymer volume fraction of (a) the correlation length ξ_S for the *solution-like* local concentration fluctuations, (b) the correlation length ξ_L for the large-scale fractal concentration fluctuations, (c) scattered intensity in the limit of zero scattering vector, and (d) relative contribution of the fractal large-scale fluctuations and the *particle* scattering to the intensity at zero scattering vector. The full lines represent linear fits to the experimental results. They imply the approximate scaling relations $\xi_L \sim \phi^{-3/2}$, $\xi_S \sim \phi^{-3/4}$, $I(q=0) \sim \phi^{-3/2}$, and $I_L(q=0)/I_S(q=0) \sim \phi^{-3/2}$. The symbol size is of the order of the larger error bar.

for the samples irradiated to doses higher than 11 Mrad. A scaling behavior is also present. A linear fit to the experimental points gave a slope of −1.49 ± 0.09, implying the approximate scaling law

$$I(q=0) \sim \phi_p^{-3/2} \tag{45}$$

Note that this is consistent with the result expected from the model used:

$$I(q=0) \sim \phi_p \xi_L^{D_L} \sim \phi_p(\phi_p^{-3/2})^{5/3} \sim \phi_p^{-3/2} \tag{46}$$

The ratio between the self-correlation and interference contributions to the intensity scattered in the limit of zero scattering vector is presented in Figure 14d as a function of polymer volume fraction in the swollen gels in a double-logarithmic plot. This ratio also scales with the polymer volume fraction for the samples cross-linked to doses higher than 11 Mrad. A linear fit to the experimental points gives a slope of −1.30 ± 0.10, implying the approximate scaling relation

$$I_i/I_p \sim \phi_p^{-4/3} \tag{47}$$

This power law agrees within the error bar with

$$I_i/I_p \sim (\xi_L/\xi_S)^{5/3} \sim \phi_p^{-5/4} \tag{48}$$

expected from the scaling between the "particle" and

interference contributions implicit in eq 37.

5. Summary and Conclusion

The results obtained lead to the conclusion that, for these networks produced by cross-linking a polydisperse melt, the molecular weight growth induced by the irradiation process is well described by the statistical approach based on the Flory–Stockmayer assumptions on the cross-linking process. Furthermore, the volume swelling upon solvent absorption is, macroscopically, qualitatively well described by the classical affine network description sufficiently far away from the gel point for the network. At the microscopic level, the results obtained from the model used to interpret small-angle neutron scattering data are summarized in a series of power laws that relate the correlation lengths ξ_L and ξ_S and the intensity scattered in the limit of zero scattering vector to the polymer volume fraction: $\xi_L \sim \phi_p^{-3/2}$, $\xi_S \sim \phi_p^{-3/4}$, $\xi_L/\xi_S \sim \phi_p^{-3/4}$, $I(q=0) \sim \phi_p^{-3/2}$, $I_L(q=0)/I_S(q=0) \sim \phi_p^{-3/2}$. Combining the power laws obtained with results from the statistical approach to the cross-linking process and from the interpretation of equilibrium swelling measurements in terms of classical models, the number of monomers in elastically effective network strands was related to the characterisetic length scale for the large-scale fluctuations in polymer density: $N_C \sim \xi_L^{3/5}$.

The volume swelling can be understood as resulting from the separation of chains at all length scales. The structure of the swollen network at large length scales was found to be well described as resulting from the establishment of some kind of excluded volume interaction between large structures including several polymers which, themselves, swell when the network goes from the dry state to maximum equilibrium swelling.

The extent to which these observations are determined by the high polydispersity present in the melt is something that is unknown and that should be investigated. We note that the power laws observed deviate from those predicted by the model of percolation clusters and also that a maximum in $I(q=0)$ as a function of cross-link density was not found. However, to resolve the two percolations predicted in the model of percolating blobs, the molecular weight in the precursor polymer should ideally be high and have a monodisperse distribution, and this is clearly not the case of the samples studied.

The work reported here on the nonextracted networks was continued by studying again as a function of cross-link density extracted samples that were measured at different swelling degrees from the dry state to maximum equilibrium swelling. The results obtained will be presented in a forthcoming paper.[55]

Acknowledgment. A.N.F. acknowledges the financial support of a C.E.C. research bursary (Contract BREU CL900378). We acknowledge many stimulating discussions with François Boué. We are grateful to Walter Batsberg for discussions concerning sample preparation, sample extraction, and GPC work and particularly grateful to Lotte Hansen for performing most of the extraction analysis and for her precious help in all the work related to the gel permeation chromatography experiments. We also thank Arne Miller and the staff of the Risø National Laboratory's 10-MeV electron accelerator for performing the irradiation of the samples.

References and Notes

(1) Flory, P. J. *Principles of Polymer Chemistry*; Cornell University Press: Ithaca, NY, 1953.
(2) Treloar, L. R. G. *The Physics of Rubber Elasticity*, 3rd ed.; Clarendon: Oxford, 1975.
(3) Dusek, K.; Prins, W. *Makromol. Chem.* **1969**, *Suppl. 2*, 87.
(4) Wall, F. T.; Flory, P. J. *J. Chem. Phys.* **1951**, *19*, 1435.
(5) James, H.; Guth, E. *J. Polym. Sci.* **1949**, *4*, 153.
(6) Flory, P. J.; Erman, B. *Macromolecules* **1982**, *15*, 800.
(7) Ball, R. C.; Doi, M.; Edwards, S. F.; Werner, M. *Polymer* **1981**, *22*, 1010.
(8) Edwards, S. F. *Br. Polym. J.* **1977**, *9*, 140.
(9) Graessley, W. W. *Adv. Polym. Sci.* **1982**, *46*, 67.
(10) Marruci, G. *Macromolecules* **1981**, *14*, 434.
(11) Gaylor, R. J. *Polym. Bull.* **1982**, *8*, 325.
(12) Mark, J. E. *Makromol. Chem.* **1979**, *Suppl. 2*, 87.
(13) Mark, J. E.; Sullivan, J. L. *J. Chem. Phys.* **1977**, *66*, 1006.
(14) Dusek, K.; Vojta, V. *Br. Polym. J.* **1977**, *9*, 164.
(15) Jacobsen, H.; Stockmayer, W. H. *J. Chem. Phys.* **1950**, *18*, 1600.
(16) Candau, S.; Bastide, J.; Delsanti, M. *Adv. Polym. Sci.* **1982**, *44*, 27.
(17) Beltzung, M.; et al. *Proc. 27th Int. Symp. Macromolecules, Strasbourg*, **1981**, 728.
(18) Duplessix, R. Thesis, Université Louis Pasteur, Strasbourg, 1975.
(19) Bastide, J.; Picot, C.; Candau, S. *J. Macromol. Sci.* **1981**, *B19*, 13.
(20) Benoit, H.; et al. *J. Polym. Sci., Polym. Phys. Ed.* **1976**, *14*, 2119.
(21) Bastide, J.; Boué, F. *Physica*, **1986**, *140A*, 251.
(22) Bastide, J.; Boué, F.; Buzier, M. *Springer Proc.Phys.* **1989**.
(23) Bastide, J.; Leibler, L. *Macromolecules*, **1988**, *21*, 2647.
(24) Bastide, J.; Mendes, E.; Boué, F.; Buzier, M.; Lindner, P. *Makromol. Chem.* **1990**, *40*, 81.
(25) Almdal, K. Risø Report Risø-M-2787(v.1), 1989.
(26) Langley, N. R. *Macromolecules* **1968**, *1*, 348.
(27) Stockmayer, W. H. *J. Chem. Phys.* **1944**, *12*, 125.
(28) Flory, P. J. *J. Am. Chem. Soc.* **1947**, *69*, 30.
(29) Charlesby, A. *Proc. R. Soc. London* **1954**, *A222*, 542.
(30) Charlesby, A. *Atomic Radiation and Polymers*; Pergamon Press: New York, 1960.
(31) Shy, L. Y.; Eichinger, B. E. *Macromolecules* **1986**, *19*, 2787.
(32) Tanny, G. B.; Pierre, L. E. *J. Phys. Chem.* **1971**, *75*, 2430.
(33) Grest, G.; Kramer, K. *J. Phys. (Paris)* **1990**, *51*, 2829.
(34) Flory, P. J. *J. Chem. Phys.* **1977**, *66*, 5720.
(35) Eichinger, B. E. *Annu. Rev. Phys. Chem.* **1983**, *34*, 359.
(36) Mark, J. E. *Adv. Polym. Sci.* **1982**, *44*, 1.
(37) Charlesby, A. *J. Polym. Sci.* **1955**, *17*, 379.
(38) St. Pierre, L. E.; Dewhurst, H. A.; Bueche, A. M. *J. Polym. Sci.* **1959**, *36*, 105.
(39) Chahal, R. S.; Kao, W. P.; Patterson, D. *J. Chem. Soc., Faraday Trans. 1* **1973**, *69*, 1834.
(40) Hauser, R.; Walker, C.; Kilbourne, F. *Ind. Eng. Chem.* **1956**, *48*, 1202.
(41) Brotzman, R. W.; Eichinger, B. E. *Macromolecules* **1981**, *14*, 1445.
(42) Flory, P. J. *Proc. R. Soc. London* **1976**, *A351*, 351.
(43) Brandrup, J.; Immergut, E. H., Eds. *Polymer Handbook*, 3rd ed.; Wiley-Interscience: New York, 1989.
(44) Scanlan, J. *J. Polym. Sci.* **1959**, *2*, 1.
(45) Graessley, W. W. *J. Polym. Sci., Polym. Phys. Ed.* **1980**, *18*, 27.
(46) Higgins, J. *Br. Polym. J.* **1987**, *19*, 103.
(47) Pedersen, J. S.; Posselt, D.; Mortensen, K. *J. Appl. Crystallogr.* **1990**, *23*, 321.
(48) de Gennes, P.-G. *Scaling Concepts in Polymer Physics*; Cornell University Press: Ithaca, NY, 1979.
(49) Mallam, S.; Horkay, F.; Hecht, A. M.; Rennie, A. R.; Geissler, E. *Macromolecules* **1991**, *24*, 543.
(50) Geissler, E.; Mallam, S.; Hecht, A. M.; Rennie, A.; Horkay, F. *Macromolecules* **1990**, *23*, 5270.
(51) Mallam, S.; Horkay, F.; Hecht, A. M.; Rennie, A. R.; Geissler, E. *J. Chem. Phys.* **1989**, *10*, 6447.
(52) Brown, W.; Mortensen, K.; Floudas, G. *Macromolecules* **1992**, *25*, 6904.
(53) Freltoft, T.; Kjems, J. K. *Phys. Rev. B* **1986**, *33*, 269.
(54) Teixeira, J. *J. Appl. Crystallogr.* **1988**, *21*, 781.
(55) Falcão, A. N.; Pedersen, J. S.; Mortensen, K.; Boué, F., to be submitted.